Supplementary Information

Rhombohedral distortion analysis of ultra-thin Pt(111) films deposited under Ar-N_2 atmosphere

Takashi Harumoto[ab]*, Takumi Sannomiya[a], Shinji Muraishi[a], Ji Shi[a] and Yoshio Nakamura[a]

[a]Department of Metallurgy and Ceramics Science, Tokyo Institute of Technology, 2-12-1-S8-6 O-okayama, Meguro-ku, Tokyo, 152-8552, Japan, and [b]Department of Materials Science and Technology, Tokyo University of Science, 6-3-1 Niijuku, Katsushika-ku, Tokyo, 125-8585, Japan

Correspondence email: taharumoto@rs.tus.ac.jp

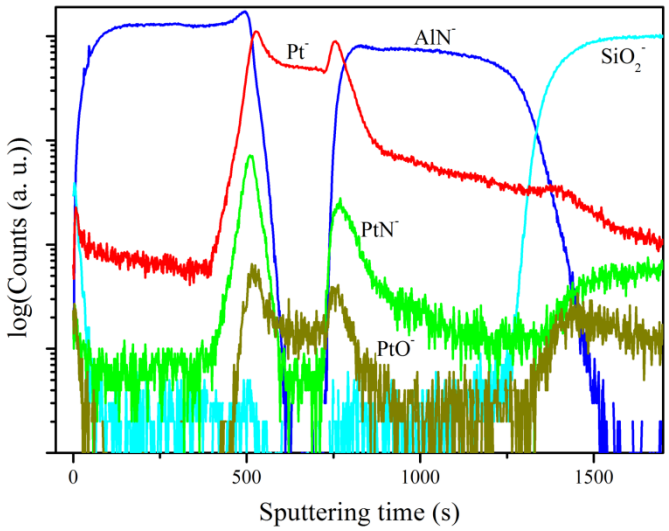

Figure S1 Depth profile of as-deposited AlN(21 nm)/Pt_{Ar}(12 nm)/AlN(21 nm)/fused silica glass measured using TOF-SIMS. The peaks at AlN/Pt and Pt/AlN interfaces are related to matrix effects and they do not indicate that the interfaces have higher density than other parts.

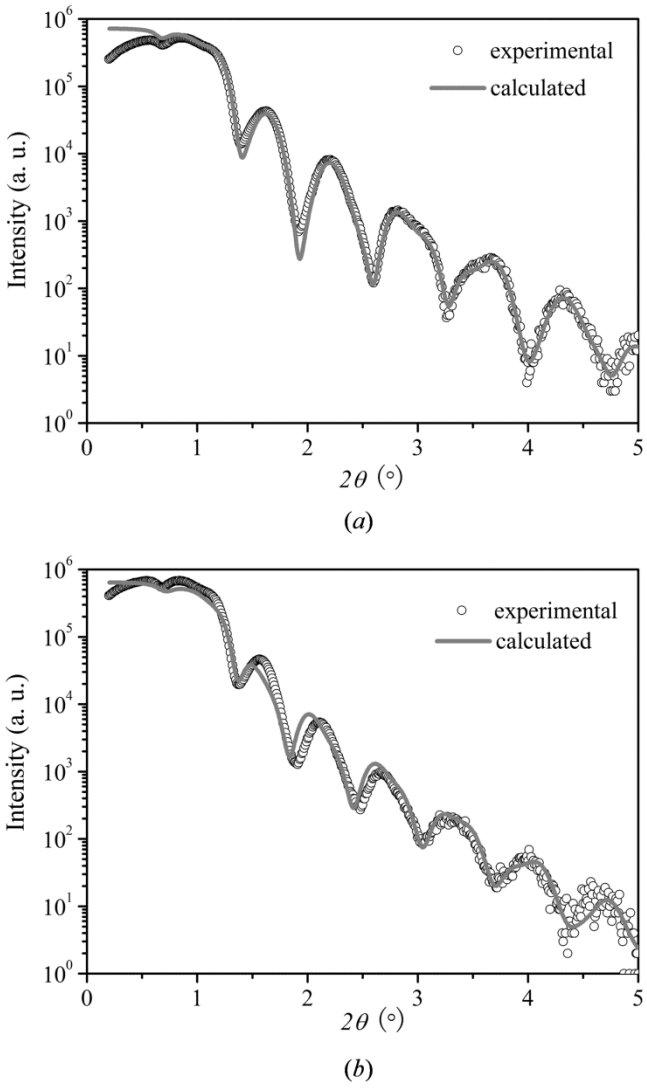

Figure S2 XRR results of AlN(16 nm)/Pt(11 nm)/AlN(16 nm)/fused silica glass of (*a*) as-deposited and (*b*) annealed at 773 K. The calculated XRR curves are also shown in the figures.

Table S1 Results of XRR curve fitting of AlN(16 nm)/Pt(11 nm)/AlN(16 nm)/fused silica glass.

	as-deposited		annealed at 773 K	
	thickness /nm	roughness /nm	thickness /nm	roughness /nm
AlN layer	16.6	0.59	14.7	0.56
Pt layer	11.5	0.45	12.6	0.54
AlN layer	16.5	0.57	13.3	0.64
fused silica glass	----	0.49	----	0.43

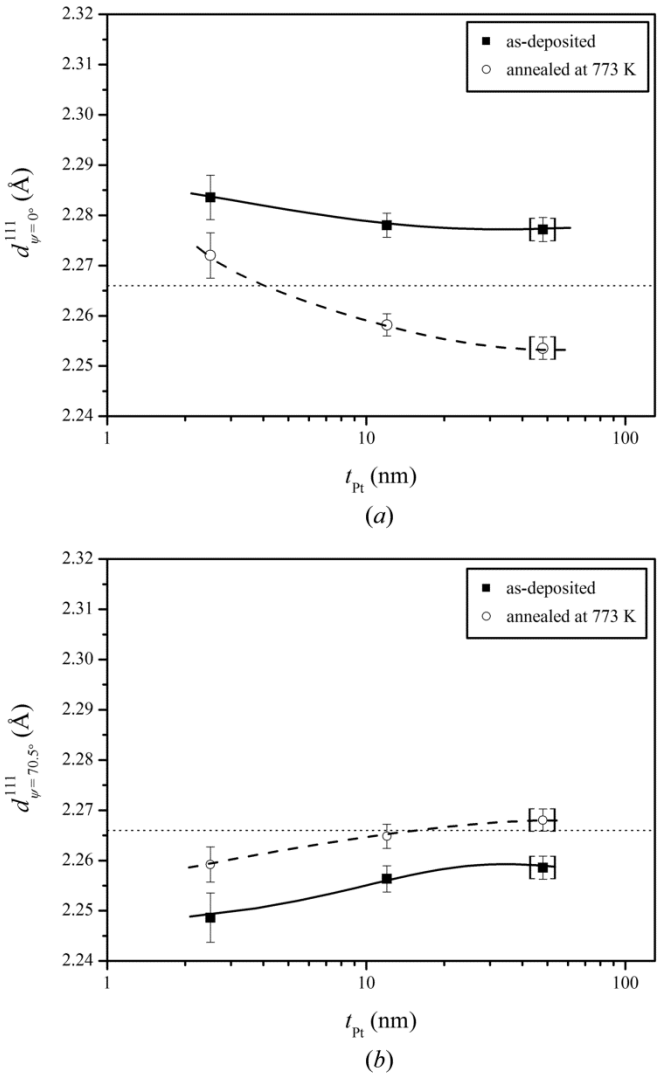

Figure S3 Thickness dependences of (*a*) $d^{111}_{\psi=0°}$ and (*b*) $d^{111}_{\psi=70.5°}$ of the ultra-thin (111)-textured Pt_{Ar} film. t_{Pt} denotes the thickness of Pt film. The plots enclosed by [ ] are the result of Pt_{Ar}/fused silica glass while others are AlN/Pt_{Ar}/AlN/fused silica glass.

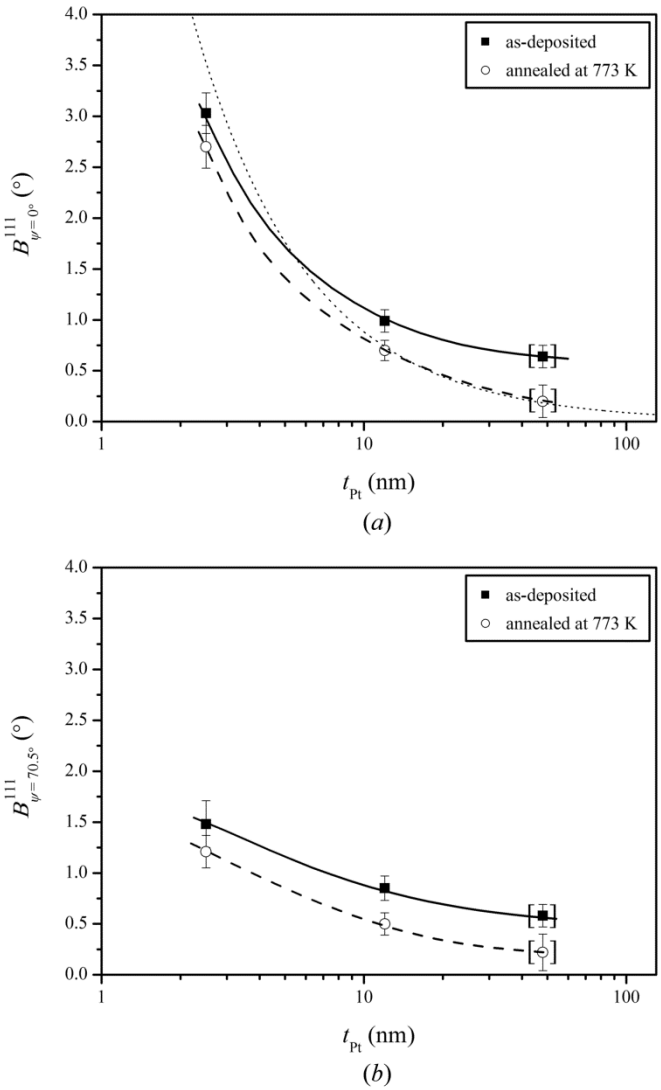

Figure S4 Thickness dependences of (*a*) $B^{111}_{\psi=0°}$ and (*b*) $B^{111}_{\psi=70.5°}$ of the ultra-thin (111)-textured Pt_{Ar} film.

The dotted line in (*a*) is a calculated result under an assumption that the perpendicular crystallite size of Pt is equal to the film thickness. The plots enclosed by [ ] are the result of Pt_{Ar}/fused silica glass while others are AlN/Pt_{Ar}/AlN/fused silica glass.

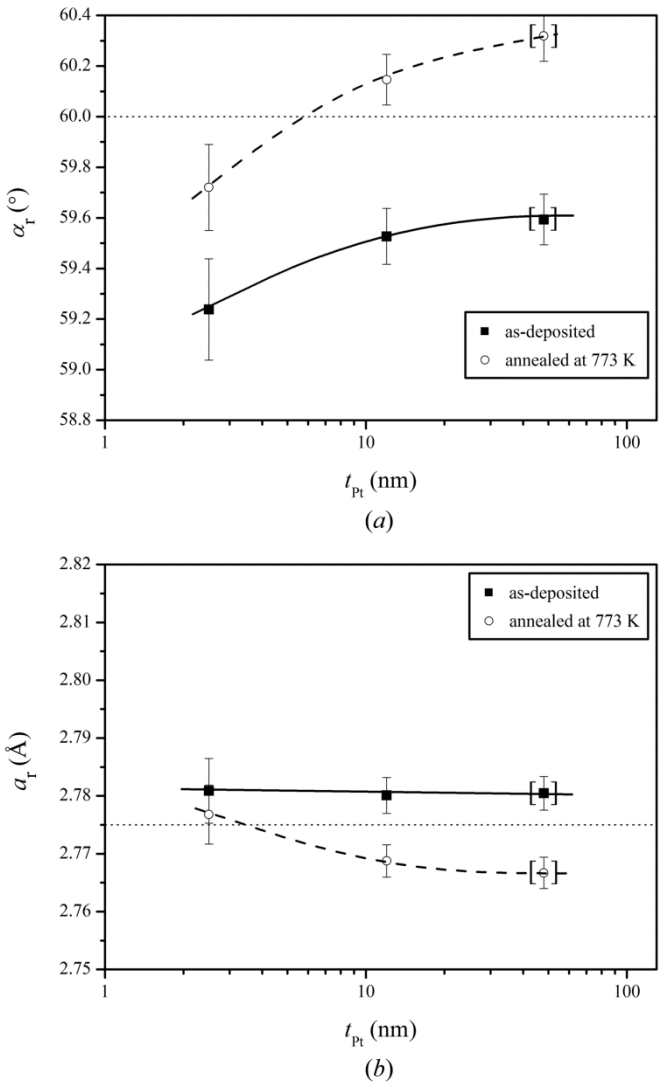

Figure S5 Results of the rhombohedral distortion analysis: thickness dependences of the primitive rhombohedral cell parameters, namely (*a*) angle and (*b*) lattice parameter, of the ultra-thin (111)-textured Pt_{Ar} film. These results are calculated from lattice spacings using equations (1) and (2). It should be noted that no elastic constant is employed for calculation. The plots enclosed by [ ] are the result of Pt_{Ar}/fused silica glass while others are AlN/Pt_{Ar}/AlN/fused silica glass.

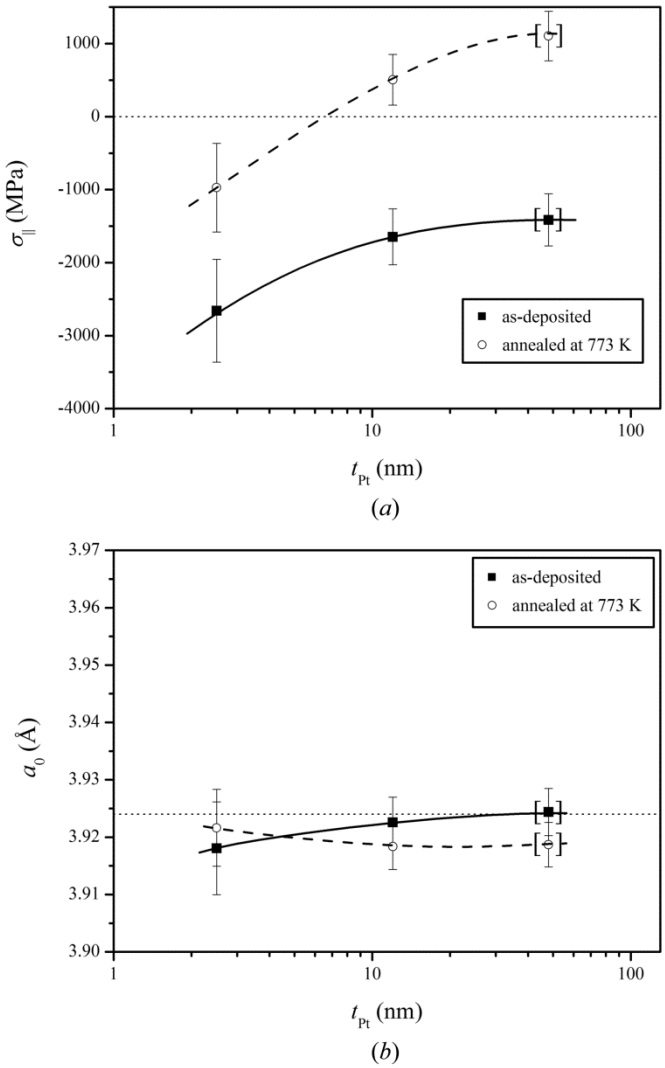

Figure S6 Results of the diffraction stress analysis: thickness dependences of (*a*) stress and (*b*) strain-free lattice parameter of the ultra-thin (111)-textured Pt_{Ar} film. These results are calculated from lattice spacings using equation (5) with the diffraction elastic constants. The same results could be calculated via the rhombohedral distortion analysis using equations (9) and (10) with the diffraction elastic constants. The plots enclosed by [ ] are the result of Pt_{Ar}/fused silica glass while others are AlN/Pt_{Ar}/AlN/fused silica glass.

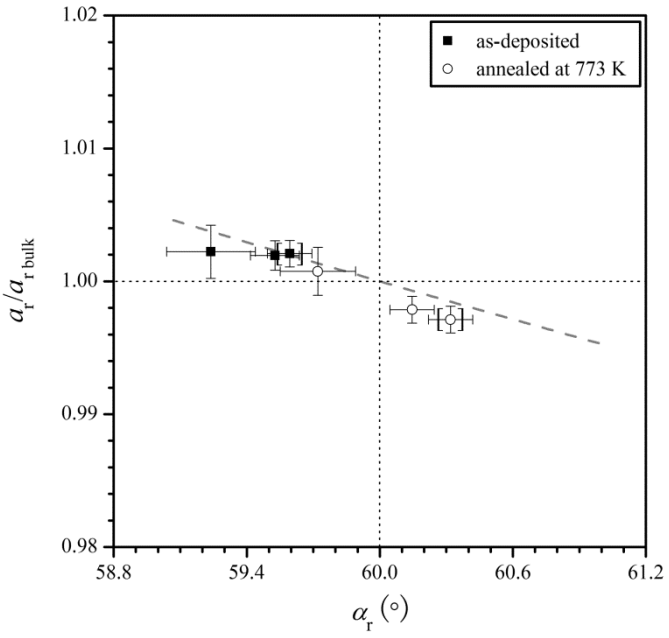

Figure S7 Results of the rhombohedral distortion analysis: (α_r, $a_r/a_{r\,bulk}$) plot of as-deposited and annealed ultra-thin (111)-textured Pt_{Ar} films. The centre point ((α_r, $a_r/a_{r\,bulk}$) = (60°, 1)) is related to the non-deformed fcc cell. The dashed grey line, which indicates the theoretical behaviour of (111)-textured Pt film under rotational symmetric biaxial stress, is calculated from equation (5) and single-crystal elastic moduli of Pt. The plots enclosed by [ ] are the result of Pt_{Ar}/fused silica glass while others are AlN/Pt_{Ar}/AlN/fused silica glass.